A Computational Framework for EEG Causal Oscillatory Connectivity

Eric Rawls   RAWLS017@UMN.EDU
Psychiatry and Behavioral Sciences
University of Minnesota

Casey Gilmore   GILMO158@UMN.EDU
Minneapolis Veterans Affairs Health Care System
Psychiatry and Behavioral Sciences
University of Minnesota

Erich Kummerfeld   ERICHK@UMN.EDU
Institute for Health Informatics
University of Minnesota

Kelvin Lim   KOLIM@UMN.EDU
Minneapolis Veterans Affairs Health Care System
Psychiatry and Behavioral Sciences
University of Minnesota

Tasha Nienow   TASHA.NIENOW@VA.GOV
Minneapolis Veterans Affairs Health Care System
Psychiatry and Behavioral Sciences
University of Minnesota

Abstract

Here we advance a new approach for measuring EEG causal oscillatory connectivity, capitalizing on recent advances in causal discovery analysis for skewed time series data and in spectral parameterization of time-frequency (TF) data. We first parameterize EEG TF data into separate oscillatory and aperiodic components. We then measure causal interactions between separated oscillatory data with the recently proposed causal connectivity method Greedy Adjacencies and Non-Gaussian Orientations (GANGO). We apply GANGO to contemporaneous time series, then we extend the GANGO method to lagged data that control for temporal autocorrelation. We apply this approach to EEG data acquired in the context of a clinical trial investigating noninvasive transcranial direct current stimulation to treat executive dysfunction following mild Traumatic Brain Injury (mTBI). First, we analyze whole-scalp oscillatory connectivity patterns using community detection. Then we demonstrate that tDCS increases the effect size of causal theta-band oscillatory connections between prefrontal sensors and the rest of the scalp, while simultaneously decreasing causal alpha-band oscillatory connections between prefrontal sensors and the rest of the scalp. Improved executive functioning following tDCS could result from increased prefrontal causal theta oscillatory influence, and decreased prefrontal alpha-band causal oscillatory influence.

Keywords: EEG, Causal Discovery, Oscillations, Traumatic Brain Injury, Transcranial Direct Current Stimulation

1. Introduction

Neural oscillations coordinate information transfer across distributed networks in the brain, providing valuable insights into brain functional organization. Oscillatory activity plays a critical role in cognitive processes (Ward, 2003), and alterations in oscillatory connectivity are implicated in numerous neurological and psychiatric disorders (Uhlhaas and Singer, 2006; Başar and Güntekin, 2008). However, brain oscillations mix with background activity that is not rhythmic. This background aperiodic activity forms a characteristic 1/f pattern in power spectra, with lowest frequencies carrying the highest power, and is potentially related to excitatory-inhibitory neurotransmitter balance in the brain (Gao et al., 2017). Aperiodic activity is a major component of electroencephalography (EEG) dynamics, and its presence can confound detection of oscillatory brain activity (Donoghue et al., 2020a; Merkin et al., 2023). Thus, methods to assess oscillatory connectivity while removing aperiodic confounding are critical for advancing our understanding of the brain's functional architecture and its relationship to cognition and behavior.

Current approaches to analyzing EEG connectivity include Granger prediction (Granger, 1969; Geweke, 1984), transfer entropy (Schreiber, 2000), and partial directed coherence (Baccalá and Sameshima, 2001). While these methods have proven valuable, they are not without limitations. For example, these prior approaches do not effectively isolate oscillatory neural activity from background aperiodic activity, which can result in aperiodic activity masking or confounding neural oscillations (Donoghue et al., 2020b,a; Merkin et al., 2023). Moreover, existing methods can suffer from the third-variable problem, where two variables that are jointly caused by a third variable can incorrectly be found to cause each other. While multivariate Granger prediction (Barnett and Seth, 2014) can address this problem, it is unable to accurately measure effect sizes of causal connectivity due to conditioning on the entire temporal history, rather than only the relevant history (Runge et al., 2019).

To address these shortcomings, we present a new framework for assessing multivariate causal oscillatory connectivity in EEG data. Our method consists of several steps. First, we apply the surface Laplacian transform (Perrin et al., 1989) to channel-level EEG data to estimate current at the surface of the dura and remove volume conduction (Nunez and Srinivasan, 2006). Second, we transform EEG data to time-frequency (TF) surfaces and parameterize the resulting TF surfaces (Donoghue et al., 2020b), separating oscillatory power from aperiodic 1/f power. Having isolated TF surfaces containing only time-varying oscillatory power estimates, we apply a multivariate causal discovery machine learning method, Greedy Adjacencies and Non-Gaussian Orientations (GANGO) (Rawls et al., 2022), to uncover causal influences between band-limited oscillatory power envelopes. We consider the case of contemporaneous time series, and we extend the GANGO method to lagged time series to statistically control for the influence of temporal autocorrelation.

Our new framework offers several advantages over current methods for EEG directed connectivity. First, by separating oscillatory and aperiodic activity, our approach minimizes the potential for confounding effects of aperiodic activity on oscillatory connectivity. Second, GANGO is amenable to skewed data distributions, providing a more appropriate analysis for heavily skewed power spectral oscillatory data. Third, GANGO utilizes a multivariate approach during network structure learning, more accurately learning global network characteristics by accounting for indirect causal relationships and third-variable

problems that can plague bivariate directed connectivity approaches. Fourth, our approach extends GANGO to lagged time series, to control for autocorrelation. Fifth, our approach does not condition on the entire history when estimating effect sizes, theoretically producing a superior estimate by comparison to Granger prediction (Runge et al., 2019).

We apply our framework to data collected during a clinical trial of noninvasive brain stimulation for mild traumatic brain injury (mTBI). We first analyze the modular community structure of our measured oscillatory connectomes. We quantify the stability of the community structures, as well as their similarity to an established non-causal connectivity method. We then examine treatment-related effects of transcranial direct current stimulation (tDCS) to the left dorsolateral prefrontal cortex (dlPFC) on the strength of causal theta- and alpha-band prefrontal connections. Our novel framework for assessing causal oscillatory connectivity in EEG data addresses key limitations of current methods, providing an accurate and comprehensive representation of causal oscillatory interactions between brain regions. By effectively separating oscillatory and aperiodic activity, accommodating skewed oscillatory data distributions, and employing a multivariate approach, our framework offers a powerful tool for advancing our understanding of the functional architecture of the human brain and the mechanisms underlying various cognitive processes.

2. Methods & Materials

2.1. Participants

Twenty nine participants enrolled in a double-blind, sham-controlled trial initiated cognitive training supplemented with either concurrent anodal tDCS targeting the DLPFC or sham stimulation. Participants were veterans enrolled at the Minneapolis VAHCS, aged 18-65, who had sustained a mild traumatic brain injury (mTBI) more than 1 year ago. Participant diagnosis of mTBI was established with a review of the medical record and administration of the Minnesota Blast Exposure Screening Tool (Nelson et al., 2011). Participants were excluded if they: had a psychotic disorder, were severely depressed, had a hospitalization or medication change in the previous 4 weeks, met criteria for substance abuse in the last month or substance dependence in the last six months, had behavioral problems preventing participation in a group intervention, had a premorbid IQ below 70, were unable to provide informed consent, had a guardian of person, had another existing neurological condition that impacts cognitive functioning, were not fluent enough in English to understand testing procedures, or have a medical condition or injury such as a lesion or open wound on their scalp that is incompatible with tDCS (Nitsche et al., 2008). All procedures were approved by ethical review boards at the Minneapolis VAHCS and the University of Minnesota.

2.2. Definition of Mild Traumatic Brain Injury

We used the definition of mTBI developed by the VA and Department of Defense and described in the document, VA/DoD Clinical Practice Guideline: Management of concussion/mild traumatic brain injury (2009). mTBI is diagnosed after reported trauma to the head due to a blunt force trauma, acceleration/deceleration forces, or exposure to blast with the following injury characteristics: 1) no structural imaging abnormalities, 2) less than 30 minutes of loss of consciousness, 3) post-traumatic amnesia lasting less than 1 day,

4) Glasgow Coma Scale (GCS) score within 24 hours of injury in the range of 13-15, and 5) alteration of consciousness/mental state for less than 24 hours.

2.3. Transcranial Direct Current Stimulation (tDCS) Protocol

Participants, trainers, and the EEG data analyst (ER) were blind to participant condition assignment. Participants in both tDCS and sham stimulation conditions received 2-3 neuromodulation sessions held on separate days each week. Sessions were approximately two hours in length, including 20 minutes of tDCS or sham stimulation concurrent with 60 minutes of cognitive training and a 45-minute strategy discussion session. A StarStim neurostimulator administered either tDCS or sham stimulation. Participants in the tDCS condition received 2 mA of stimulation with the anodal electrode placed over F3 (left DLPFC), and the cathodal electrode placed in the contralateral supraorbital position. Current was induced through two circular carbon rubber core electrodes in saline-soaked sponges (25 cm^2), placed in a neoprene headcap with marked locations based on the 10-10 EEG system. These are all common stimulation parameters for treatment of psychiatric conditions (Li et al., 2022) and none of the participants reported adverse effects or discomfort associated with stimulation. Participants who were in the sham condition received 30 seconds of stimulation to mimic the experience of tDCS. This protocol is recommended for blinded tDCS administration (Giglia et al., 2011).

2.4. EEG Collection and Preprocessing

Resting-state EEG was collected at three time points: 1) at baseline, prior to the first tDCS training session (EEG Baseline), 2) immediately after the first training session (EEG Session 1), and 3) following the complete course of 24 intervention sessions (EEG Session 2). Participants sat quietly with eyes closed while continuous EEG were recorded for three minutes using a 32-channel BioSemi ActiveTwo system. Data were preprocessed using EEGLAB (Delorme and Makeig, 2004). Following data preparation, we selected the first one minute (15,000 samples at 250 Hz) of recording without voltage exceeding ±100 μV for further processing. We high-pass filtered the data at 0.5 Hz, low-pass filtered the data at 40 Hz, calculated independent components analysis (ICA) (Makeig et al., 1996), and removed artifact components using ICLabel (Pion-Tonachini et al., 2019).

2.5. EEG Time-frequency Analysis and Parameterization

We applied the surface Laplacian transformation (Perrin et al., 1989), attenuating volume conduction. While some prior approaches have used inverse source reconstruction, source localization with such sparse montages (32 channels) is associated with high localization errors and large remaining volume conduction artifacts (Song et al., 2015). Instead, we calculate channel-level connectivity, a common approach for EEG connectivity (Miskovic et al., 2015). TF transformation used the lead author's NeuroFreq toolbox (https://github.com/erawls-neuro/NeuroFreq_public. We transformed the EEG to a TF representation using short time Fourier transform (STFTs) with a one second Hamming window, 80% overlap, and averaging of three adjacent segments to increase signal-to-noise ratio. These are very similar parameters to those reported to produce high-quality results in (Wilson et al., 2022) and are common parameters for TF analysis (Keil et al., 2022), as well

as enabling accurate resolution of all frequencies of interest because a 1-s window produces a Rayleigh frequency (lowest measurable frequency) of 1 Hz. This analysis returned 29 frequencies spanning approximately 1.95 Hz to 29.3 Hz and 300 time points sampled every 200 ms. We followed the approach outlined in (Wilson et al., 2022) to parameterize each time-resolved power spectrum using default parameters from specparam (peak widths = [0.5 12], peak detection threshold = 2.0 SD, no max number of peaks, no minimum peak height, aperiodic mode = fixed) (Donoghue et al., 2020b). TF parameterization used BrainStorm software (Tadel et al., 2011). We averaged the parameterized oscillatory power into two canonical frequency bands (theta = 3.91-7.81 Hz, alpha = 8.79-13.67 Hz) for causal oscillatory connectivity analyses. For a visual comparison of total (unparameterized), aperiodic, and oscillatory power estimates, see Figure 1.
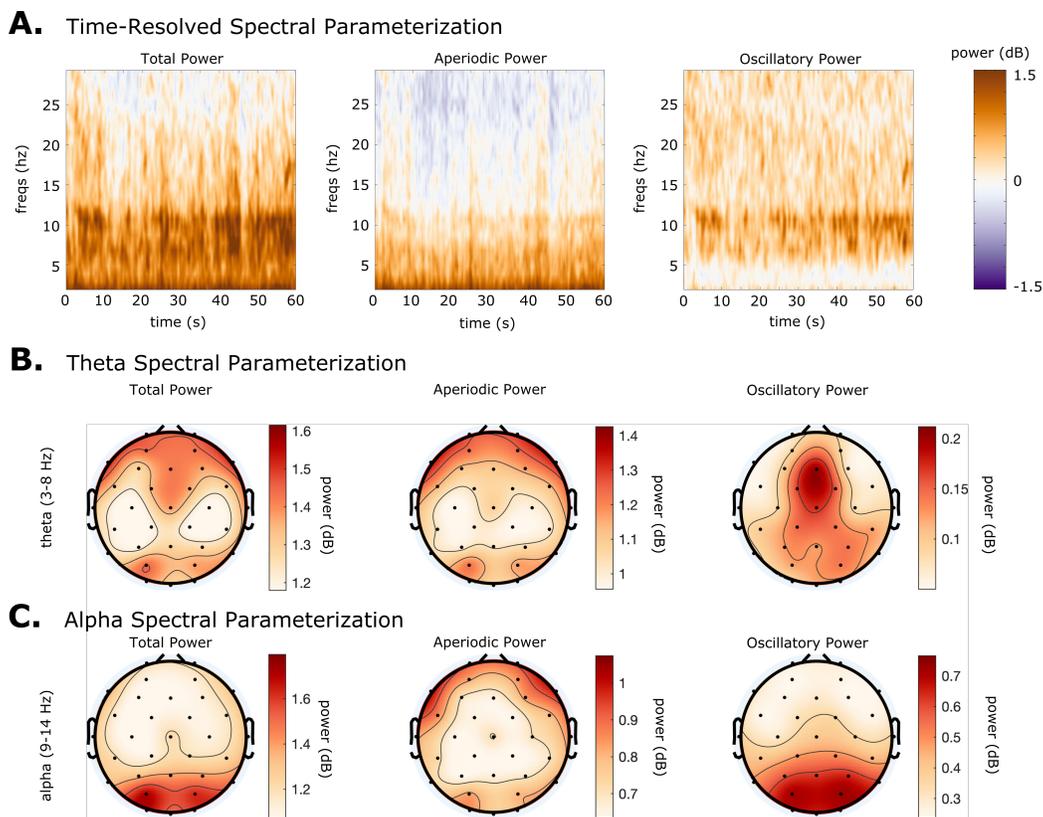

Figure 1: Laplacian-transformed TF data were parameterized to separate aperiodic and oscillatory contributions. **A.** Panels illustrate spectral parameterization for a single participant, averaged over all channels. **B.** Panels represent the average of theta-band total, aperiodic, and oscillatory spectral power. Note the enhanced spatial focus of oscillatory theta power over mediofrontal sensors. **C.** Panels represent the average of alpha-band total, aperiodic, and oscillatory spectral power. Note the enhanced spatial focus of oscillatory alpha power over posterior sensors.

2.6. EEG Causal Connectivity Analysis

We generated individualized causal oscillatory connectomes using GANGO (Greedy Adjacencies and Non-Gaussian Orientations), a causal discovery method we proposed in (Rawls et al., 2022). We initially developed this method to be suitable for resting-state fMRI data, so we tested whether our resting-state oscillatory EEG met the assumptions of the GANGO algorithm - specifically, skewness with reference to Gaussian data. We simulated Gaussian data and tested whether the observed EEG data passed the 95th percentile of the skewness of the surrogate Gaussian data. Following assumption checks, we calculated individualized causal connectomes as described in (Rawls et al., 2022). We used causal-cmd (Version 1.3.0; https://github.com/bd2kccd/causal-cmd) to generate data-driven connectomes with Fast Greedy Equivalence Search (FGES). FGES includes a penalty term, which we set to 1 for consistency with our previous work (Rawls et al., 2022; Camchong et al., 2022) and because a penalty discount of 1 corresponds to the standard Bayesian Information Criterion (Schwarz, 1978). We then used a robust skewness-based method to reorient the edges (Hyvärinen and Smith, 2013). For more details on the GANGO algorithm see (Rawls et al., 2022). Following structure learning, we fit structural equation models (SEMs) using semopy (Igolkina and Meshcheryakov, 2020) to each causal connectome to recover standardized effect sizes for each causal connection (Camchong et al., 2022). Here, we consider both the original GANGO method which does not consider temporal information (Rawls et al., 2022), as well as documenting an extension of the GANGO method that factors out effects of temporal autocorrelation. This is achieved by conditioning on the entire set of observed variables with a temporal lag, which as noted by (Ramsey et al., 2010) statistically removes the impact of autocorrelation even when the causal relationship is undersampled. First, we apply FGES with tiered knowledge forbidding back-in-time causality. Then, having learned each contemporaneous variables time-lagged direct causes, we regress these time-lagged direct causes out and apply robust skew-based reorientation to the residuals. In the following, we present results calculated using both approaches.

2.7. EEG Magnitude-Squared Coherence Connectivity Analysis

For comparison to causal connectomes, we used magnitude-squared coherence (MSC) (Nunez et al., 1997), often simply called coherence, a field-standard approach to measuring EEG connectivity that produces undirected connectomes. MSC requires only the parameters used for short-time Fourier transform, which we set to the same values as the causal connectivity analysis for consistency (one second Hamming windows and 80% segment overlap). MSC was calculated using the MATLAB function mscohere. We thresholded the continuous coherence values to include the n strongest edges where n is equal to the number of edges in the individual's causal connectome. MSC must be applied to raw time series as it first calculates STFT then measures coherence using both power and phase, while spectral parameterization at present applies only to power spectra (not phase) (Donoghue et al., 2020b). Thus, since MSC cannot be applied to parameterized EEG oscillations it could suffer from contamination by aperiodic activity, a problem specifically solved by our proposed framework. Note that this comparison is not intended to show "correctness" of the proposed approach, but instead to quantitatively assess the similarity of the resulting connectomes with those produced by a field-standard method.

2.8. Louvain Modularity Analysis

We examined the community structure of theta and alpha oscillatory causal connectomes using Louvain community detection (Blondel et al., 2008). We used the approach outlined in a recent fMRI network analysis (Ji et al., 2019). Specifically, we applied the Louvain algorithm to the weighted adjacency matrix (averaged over all participants/sessions) with 1000 repetitions. We calculated the similarity of each individual partition with each other partition using the Adjusted Rand Index (ARI) (Hubert and Arabie, 1985), an empirical measure of cluster similarity. Finally, we selected as representative the partition that showed the highest mean ARI with all other partitions. We ran this same analysis for MSC connectomes. We characterize these community structures in several ways. First, we compared network structures between unlagged, lagged, and MSC connectomes quantitatively using ARI. We tested whether these similarity metrics were more similar than expected under chance using permutation testing that randomized the community structures every run (1000 runs) to estimate a null distribution of similarity values. Second, we compared the stability of community structures estimated using our framework to the stability of MSC communities by comparing pairwise ARIs from all 1000 Louvain runs using a Mann-Whitney U test. Together, these analyses allow us to determine 1) whether our framework returns community partitions that are similar to previously described results, 2) whether the community affiliations measured from our framework are more stable over repeated Louvain runs than those returned by MSC, and 3) whether the community affiliations measured from our framework are more similar than expected by chance to those returned by MSC.

2.9. Effects of Noninvasive Brain Stimulation - EEG Connectivity Metrics

Our analysis of brain stimulation effects focused on causal connectivity edge effect sizes (measured via SEM) of a cluster of sensors including and immediately surrounding the stimulation site, F3 (included sensors: F3, AF3, F7, FC5, FC1, Fz). GANGO provides separate estimates of the presence of incoming and outgoing causal connections, as well as the sign (positive or negative) of those edges. Thus, we ran separate analyses examining the edge strength of incoming/outgoing and positive/negative edges. Our primary analysis focused on lateral prefrontal connectivity with all other scalp sensors as an average measure of prefrontal brain connectivity strength. We applied the surface Laplacian transform to the EEG data, modeling out volume conduction effects. Nevertheless, our 32-channel montage is at the low end of what is recommended for surface Laplacian analysis so it is possible some volume conduction could remain in the data. Thus we examined average prefrontal causal connectivity with a cluster of parietal-occipital sensors that were spatially separated by at least one sensor from the prefrontal cluster (included sensors: P7, CP5, P3, PO3, CP1, Pz, O1, Oz, O2, P8, CP2, P4, PO4, CP6, O2). This separation further reduces the likelihood of volume conduction impacting our results. For comparison, we examined prefrontal MSC in the same way. For an illustration of the channel clusters see Figure 4. We calculated prefrontal causal connectivity averages for each participant and session (baseline, post-treatment 1, post-treatment 2) separately, and exported these estimates for statistical analysis.

2.10. Statistical Analysis

Statistical analyses were conducted in R (version 4.1.1). We examined averaged prefrontal band-limited oscillatory causal connectivity using restricted maximum likelihood (REML)-based Mixed Model Repeated Measures (MMRMs), which outperform imputation methods for clinical trial designs with missing data (Siddiqui, 2011; Ashbeck and Bell, 2016). We ran MMRMs using generalized least squares fit with nlme (Version 3.1-161). Within-patient errors used an unstructured (co)variance matrix shared across treatment groups. We conducted separate MMRMs modeling Treatment (stim/sham) X Session (session 1/session 2) effects for incoming/outgoing and positive/negative prefrontal connection strengths. All models estimated treatment effects while covarying for baseline (Session 0) connectivity. We assessed significance using type III F-tests. Significant model effects were characterized using emmeans (Version 1.8.4-1) with Satterthwaite's approximation to correct post hoc degrees of freedom. We focus on main effects of Treatment that do not interact with Session, since these main effects indicate long-lasting connectivity changes following treatment.

3. Results

3.1. EEG Oscillatory Time Series Meet Assumptions for Causal Connectivity Analysis

Across all participants, sessions, sensors, and frequency bands (total n = 9728), every single time series was significantly more skewed ($p < .05$) than surrogate Gaussian data. All skews were positive, avoiding potential pitfalls of skew-based reorientation mentioned in (Hyvärinen and Smith, 2013). As such, the parameterized oscillatory data meet the assumptions of the GANGO method (Figure 2).
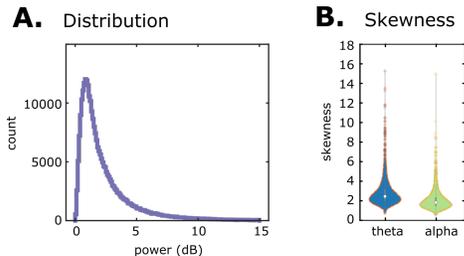

Figure 2: Following removal of aperiodic contributions, oscillatory power spectra were statistically skewed in all frequency bands, for each participant, session, and channel. **A:** Distribution of oscillatory power values for one randomly-chosen participant. **B:** Skewness values for theta and alpha oscillatory power, for all participants, sessions, and channels.

3.2. The Causal Oscillatory Community Structure of Resting-State EEG

For theta-band causal oscillatory connectivity, Louvain modularity analysis revealed four functional modules for both contemporaneous and time-lagged connectomes. These mod-

ules were dominated by a large frontal network that was identical across lagged and un-lagged connectomes. Both connectomes additionally showed a central module and right- and left-lateralized parietal-occipital modules. (Figure 3). Applying this same analysis to the MSC connectomes demonstrated a network partition with three modules: a large prefrontal module and two lateralized central-parietal-occipital modules. The unlagged and lagged connectomes were more similar than expected by chance (ARI = 0.77, p < .001), implying that autocorrelation did not fundamentally confound our network estimations. Lagged and unlagged causal connectomes were both more similar to MSC connectomes than expected by chance (lagged ARI = 0.57, unlagged ARI = 0.64, both p < .001). Considering stability over repeated decompositions, unlagged connectomes had a mean pairwise ARI of 0.99, and lagged connectomes had a mean pairwise ARI of 0.88. MSC had an ARI of 0.70 over repeated runs, significantly less stable than both lagged and unlagged causal connectomes (both Z > 40, p < .001).

For alpha-band causal oscillatory connectivity, Louvain modularity analysis revealed six functional modules for both contemporaneous and time-lagged connectomes. These modules showed central, right and left parietal-occipital, and right-central modules across both lagged and unlagged connectomes. Lagged and unlagged connectomes showed slight differences in the location and lateralization of frontal modules (Figure 3). Applying this same analysis to the MSC connectomes demonstrated a network partition with four functional modules: a single bilateral frontal network, a single central network, and two lateralized parietal-occipital networks. The unlagged and lagged connectomes were more similar than expected by chance (ARI = 0.74, p < .001), implying that autocorrelation did not fundamentally confound our network estimations. Lagged and unlagged causal connectomes were both more similar to MSC connectomes than expected by chance (lagged ARI = 0.31, unlagged ARI = 0.28, both p < .001). Considering stability over repeated decompositions, unlagged connectomes had a mean pairwise ARI of 0.82, and lagged connectomes had a mean pairwise ARI of 0.998. MSC had an ARI of 0.97 over repeated runs, significantly more stable than unlagged causal connectomes, but significantly less stable than lagged causal connectomes (both $|Z| > 35$, p < .001).

Overall, our analysis of causal oscillatory connectivity returns connectomes with a modular community structure. Our causal connectomes are quantitatively similar to connectomes based on classical methods (MSC). Results from stability analysis generally favored causal connectomes over undirected connectomes. Relative to classical methods theta-band oscillatory causal connectomes had improved stability for both lagged and unlagged connectomes, while alpha-band oscillatory causal connectomes had decreased stability for unlagged connectomes but increased stability for lagged connectomes.

3.3. tDCS Noninvasively Rewires Prefrontal Causal Connectivity

We examined effects of Treatment (stim/sham) and Session (post-treatment session 1, post-treatment session 2) on EEG causal oscillatory connectivity effect sizes, while controlling for pre-treatment causal connectivity estimates. Results are summarized in Table 1 and in Figure 4. All causal connectomes (lagged/unlagged/theta/alpha) showed significant effects of Treatment (Table 1).

A. Unlagged Theta   **B.** Lagged Theta   **C.** MSC Theta   **D.** Pairwise ARI

	Unlagged	Lagged	MSC
	0.99	0.77	0.64
	0.77	0.88	0.57
	0.64	0.57	0.70

E. Unlagged Alpha   **F.** Lagged Alpha   **G.** MSC Alpha   **H.** Pairwise ARI

	Unlagged	Lagged	MSC
	0.82	0.74	0.28
	0.74	0.998	0.31
	0.28	0.31	0.97
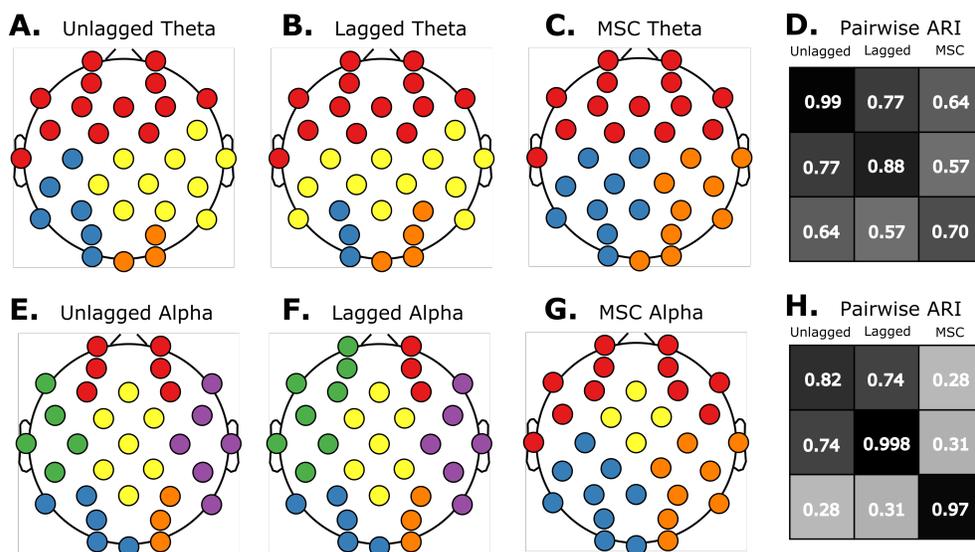
Figure 3: The causal oscillatory community structure of resting-state EEG. **A:** Unlagged theta-band communities revealed by our causal connectivity framework. **B:** Time-lagged theta-band communities revealed by our causal connectivity framework. **C:** Theta-band communities revealed by MSC. **D:** Pairwise ARI values comparing theta community structures for different network learning approaches. **E:** Unlagged alpha-band communities revealed by our causal connectivity framework. **F:** Time-lagged alpha-band communities revealed by our causal connectivity framework. **G:** Alpha-band communities revealed by MSC. **H:** Pairwise ARI values comparing alpha community structures for different network learning approaches.

	Unlagged	Lagged
Theta-Incoming	$F(1,39) = 4.71$, p = .036* $t(14.1) = $ **2.17**, p = **.047***	$F(1,39) = 4.02$, p = .052ˆ $t(14.1) = 2.00$, p = .063ˆ
Theta-Outgoing	n.s. n.s.	$F(1,39) = 4.73$, p = .036* $t(17.6) = $ **2.18**, p = **.044***
Alpha-Incoming	$F(1,39) = 6.61$, p = .014* $t(17) = $ **-2.57**, p = **.020***	n.s. n.s.
Alpha-Outgoing	n.s. n.s.	n.s. n.s.

Table 1: Summary of statistical tests for Treatment effects on causal oscillatory connectivity. F-tests reflect main MMRM effects, while t-statistics reflect post hoc estimated marginal means. Note that the signs of post hoc testing differ for theta and alpha, reflecting Treatment-related increases in theta connectivity and decreases in alpha connectivity. * = p < .05, ˆ = p < .10, n.s. = not significant (p > .10).

For unlagged theta-band connectomes, Treatment effect included increased prefrontal causal indegree weights from parietal/occipital sensors. For lagged theta connectomes, this Treatment effect was present at a trend level, in addition to treatment-related increases in prefrontal causal outdegree weights to parietal/occipital sensors. All increases were seen in the Stim group compared to the Sham group, consistent with an effect of tDCS strengthening both incoming and outgoing prefrontal theta causal connections.

For unlagged alpha-band connectomes, Treatment effect included decreased prefrontal causal indegree weights from parietal/occipital sensors for stim (compared to sham), consistent with an effect of tDCS weakening incoming alpha connections. For lagged alpha connectomes, this Treatment effect did not replicate (Figure 4).
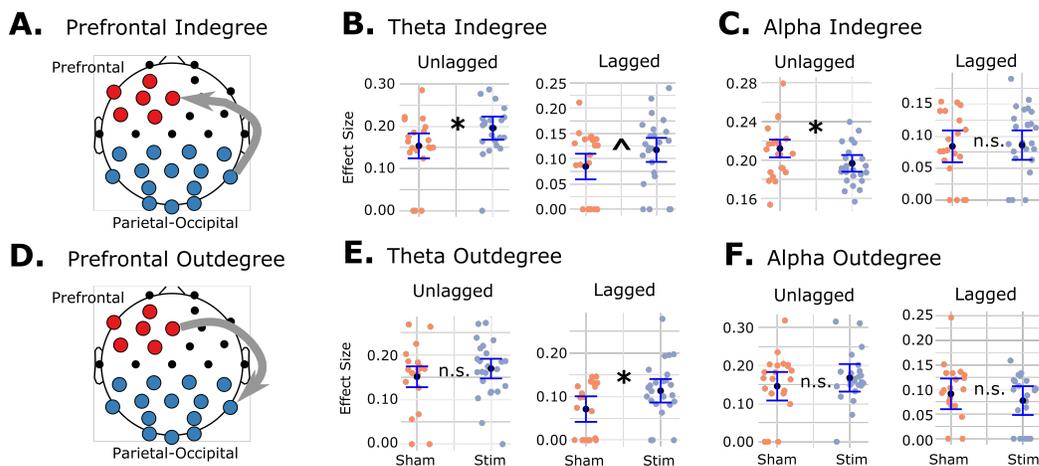
Figure 4: tDCS treatment effects on causal oscillatory connectivity. **A:** Sensor clusters for analyses, depicting prefrontal indegree. Prefrontal sensors (red) were used as seed regions for all analyses. **B:** tDCS increased the average strength of incoming theta-band positive causal connections from prefrontal sensors, both with and without controlling for autocorrelation using a time lag. **C:** tDCS decreased the average strength of incoming alpha connections, but not when data contained a time lag that controlled for autocorrelation. **D:** Sensor clusters for analyses, depicting prefrontal outdegree. **E:** tDCS increased the average strength of outgoing connections for theta data when using a time lag controlling for autocorrelation. **C:** tDCS did not impact alpha connectomes when controlling for autocorrelation using a time lag. * = p < .05, ˆ = p < .10, n.s. = not significant (p > .10).

We did not observe any significant Treatment effects for connections other than positive edges. In a control analysis using MSC, a standard undirected measure of connectivity, we did not observe any significant Treatment effects in any frequency band. As such, only our causal analysis of tDCS effects on prefrontal causal oscillatory connectivity revealed that noninvasive prefrontal brain stimulation upregulates the strength of theta-band oscillatory connections from the stimulated area of PFC, while simultaneously downregulating the strength of alpha-band causal oscillatory connectivity in the same area.

4. Discussion

This appears to be the first framework that estimates causal connectivity in EEG following removal of aperiodic contributions which can confound EEG oscillatory measurements (Merkin et al., 2023; Donoghue et al., 2020a). The modular structure of resting-state causal oscillatory connectivity was more stable than that of field-standard coherence (Nunez et al., 1997), particularly when controlling for autocorrelation using time-lagged data. Brain stimulation led to increased strength of incoming prefrontal theta connections, and to decreased strength of outgoing alpha-band connections. When controlling for autocorrelation, we noted stimulation-related increases in outgoing theta-band effect sizes, while controlling for autocorrelation reduced alpha-band effects to non-significance. This suggests that non-invasive brain stimulation can modulate these frequencies in a targeted manner. Future work will tie these neurophysiological modulations to cognitive outcomes, informing the development of personalized tDCS protocols for cognitive enhancement. Limitations to be addressed by future work include validating our framework using simulations with a known ground-truth network oscillatory connectivity pattern, incorporating individualized alpha and theta frequency band definitions (Klimesch, 1999), estimating total causal effects which include indirect and direct effects (Runge et al., 2019) rather than only the direct effects presented here, and including more than one time lag to estimate long-memory neural causal effects that cross multiple temporal lags. In summary, we demonstrate a new framework measuring causal EEG oscillatory connectivity. The method and findings enhance our understanding of the neurophysiological mechanisms underlying noninvasive brain stimulation, providing valuable insights for the design and implementation of tDCS protocols in therapeutic contexts.

Data and Code Availability

Data access requires a data use agreement with the Minneapolis VAHCS. All toolboxes used are publicly available. EEG preprocessing used the EEGLAB toolbox (https://github.com/sccn/eeglab), EEG time-frequency analysis used the lead author's NeuroFreq toolbox (https://github.com/erawls-neuro/NeuroFreq_public), and TF parameterization used the BrainStorm toolbox (https://github.com/brainstorm-tools/brainstorm3).

Causal discovery analysis used the causal-cmd program (https://github.com/bd2kccd/causal-cmd) which calls Tetrad routines (https://github.com/cmu-phil/tetrad), and non-Gaussian pairwise reorientation of contemporaneous edges used code made available by A. Hyvärinen (https://www.cs.helsinki.fi/u/ahyvarin/code/pwcausal/). Future versions of the NeuroFreq toolbox will incorporate code to automate these causal oscillatory connectivity analyses.

References

Erin L. Ashbeck and Melanie L. Bell. Single time point comparisons in longitudinal randomized controlled trials: power and bias in the presence of missing data. *BMC Medical Research Methodology*, 16(1):43, April 2016. ISSN 1471-2288. doi: 10.1186/s12874-016-0144-0. URL https://doi.org/10.1186/s12874-016-0144-0.

L. A. Baccalá and K. Sameshima. Partial directed coherence: a new concept in neural structure determination. *Biological Cybernetics*, 84(6):463–474, June 2001. ISSN 0340-1200. doi: 10.1007/PL00007990.

Lionel Barnett and Anil K Seth. The mvgc multivariate granger causality toolbox: a new approach to granger-causal inference. *Journal of neuroscience methods*, 223:50–68, 2014.

Erol Başar and Bahar Güntekin. A review of brain oscillations in cognitive disorders and the role of neurotransmitters. *Brain Research*, 1235:172–193, October 2008. ISSN 0006-8993. doi: 10.1016/j.brainres.2008.06.103. URL https://www.sciencedirect.com/science/article/pii/S0006899308015473.

Vincent D. Blondel, Jean-Loup Guillaume, Renaud Lambiotte, and Etienne Lefebvre. Fast unfolding of communities in large networks. *Journal of Statistical Mechanics: Theory and Experiment*, 2008(10):P10008, October 2008. ISSN 1742-5468. doi: 10.1088/1742-5468/2008/10/P10008. URL https://doi.org/10.1088%2F1742-5468%2F2008%2F10%2Fp10008. Publisher: IOP Publishing.

Jazmin Camchong, Mark Fiecas, Casey S. Gilmore, Matt Kushner, Erich Kummerfeld, Bryon A. Mueller, Donovan Roediger, and Kelvin O. Lim. Frontal tDCS reduces alcohol relapse rates by increasing connections from left dorsolateral prefrontal cortex to addiction networks, November 2022. URL https://www.medrxiv.org/content/10.1101/2022.11.28.22282521v1. ISSN: 2228-2521 Pages: 2022.11.28.22282521.

Arnaud Delorme and Scott Makeig. Eeglab: an open source toolbox for analysis of single-trial eeg dynamics including independent component analysis. *Journal of neuroscience methods*, 134(1):9–21, 2004.

Thomas Donoghue, Julio Dominguez, and Bradley Voytek. Electrophysiological Frequency Band Ratio Measures Conflate Periodic and Aperiodic Neural Activity. *eNeuro*, 7(6): ENEURO.0192–20.2020, December 2020a. ISSN 2373-2822. doi: 10.1523/ENEURO.0192-20.2020. URL https://www.ncbi.nlm.nih.gov/pmc/articles/PMC7768281/.

Thomas Donoghue, Matar Haller, Erik J. Peterson, Paroma Varma, Priyadarshini Sebastian, Richard Gao, Torben Noto, Antonio H. Lara, Joni D. Wallis, Robert T. Knight, Avgusta Shestyuk, and Bradley Voytek. Parameterizing neural power spectra into periodic and aperiodic components. *Nature neuroscience*, 23(12):1655–1665, December 2020b. ISSN 1097-6256. doi: 10.1038/s41593-020-00744-x. URL https://www.ncbi.nlm.nih.gov/pmc/articles/PMC8106550/.

Richard Gao, Erik J Peterson, and Bradley Voytek. Inferring synaptic excitation/inhibition balance from field potentials. *Neuroimage*, 158:70–78, 2017.

John F. Geweke. Measures of Conditional Linear Dependence and Feedback between Time Series. *Journal of the American Statistical Association*, 79(388):907–915, December 1984. ISSN 0162-1459. doi: 10.1080/01621459.1984.10477110. URL https://www.tandfonline.com/doi/abs/10.1080/01621459.1984.10477110. Publisher: Taylor & Francis _eprint: https://www.tandfonline.com/doi/pdf/10.1080/01621459.1984.10477110.

G. Giglia, P. Mattaliano, A. Puma, S. Rizzo, B. Fierro, and F. Brighina. Neglect-like effects induced by tDCS modulation of posterior parietal cortices in healthy subjects. *Brain Stimulation*, 4(4):294–299, October 2011. ISSN 1876-4754. doi: 10.1016/j.brs.2011.01.003.

C. W. J. Granger. Investigating Causal Relations by Econometric Models and Cross-spectral Methods. *Econometrica*, 37(3):424–438, 1969. ISSN 0012-9682. doi: 10.2307/1912791. URL https://www.jstor.org/stable/1912791. Publisher: [Wiley, Econometric Society].

Lawrence Hubert and Phipps Arabie. Comparing partitions. *Journal of Classification*, 2(1):193–218, 1985. ISSN 1432-1343. doi: 10.1007/BF01908075. URL https://doi.org/10.1007/BF01908075.

Aapo Hyvärinen and Stephen M. Smith. Pairwise Likelihood Ratios for Estimation of Non-Gaussian Structural Equation Models. *Journal of machine learning research: JMLR*, 14(Jan):111–152, January 2013. ISSN 1532-4435.

Anna A. Igolkina and Georgy Meshcheryakov. semopy: A Python Package for Structural Equation Modeling. *Structural Equation Modeling: A Multidisciplinary Journal*, 27(6):952–963, November 2020. ISSN 1070-5511. doi: 10.1080/10705511.2019.1704289. URL https://doi.org/10.1080/10705511.2019.1704289. Publisher: Routledge _eprint: https://doi.org/10.1080/10705511.2019.1704289.

Jie Lisa Ji, Marjolein Spronk, Kaustubh Kulkarni, Grega Repovš, Alan Anticevic, and Michael W. Cole. Mapping the human brain's cortical-subcortical functional network organization. *NeuroImage*, 185:35–57, January 2019. ISSN 10538119. doi: 10.1016/j.neuroimage.2018.10.006. URL https://linkinghub.elsevier.com/retrieve/pii/S1053811918319657.

Andreas Keil, Edward M Bernat, Michael X Cohen, Mingzhou Ding, Monica Fabiani, Gabriele Gratton, Emily S Kappenman, Eric Maris, Kyle E Mathewson, Richard T

Ward, et al. Recommendations and publication guidelines for studies using frequency domain and time-frequency domain analyses of neural time series. *Psychophysiology*, 59 (5):e14052, 2022.

W. Klimesch. EEG alpha and theta oscillations reflect cognitive and memory performance: a review and analysis. *Brain Research Reviews*, 29(2):169–195, April 1999. ISSN 0165-0173. doi: 10.1016/S0165-0173(98)00056-3. URL http://www.sciencedirect.com/science/article/pii/S0165017398000563.

Qing Li, Yu Fu, Chang Liu, and Zhiqiang Meng. Transcranial direct current stimulation of the dorsolateral prefrontal cortex for treatment of neuropsychiatric disorders. *Frontiers in Behavioral Neuroscience*, 16:893955, 2022.

Scott Makeig, Anthony J Bell, Tzyy-Ping Jung, and Terrence J Sejnowski. Independent Component Analysis of Electroencephalographic Data. *Advances in Neural Information Processing Systems*, page 7, 1996.

Ashley Merkin, Sabrina Sghirripa, Lynton Graetz, Ashleigh E. Smith, Brenton Hordacre, Richard Harris, Julia Pitcher, John Semmler, Nigel C. Rogasch, and Mitchell Goldsworthy. Do age-related differences in aperiodic neural activity explain differences in resting EEG alpha? *Neurobiology of Aging*, 121:78–87, January 2023. ISSN 0197-4580. doi: 10.1016/j.neurobiolaging.2022.09.003. URL https://www.sciencedirect.com/science/article/pii/S0197458022002019.

Vladimir Miskovic, Xinpei Ma, Chun-An Chou, Miaolin Fan, Max Owens, Hiroki Sayama, and Brandon E Gibb. Developmental changes in spontaneous electrocortical activity and network organization from early to late childhood. *Neuroimage*, 118:237–247, 2015.

Nathaniel W. Nelson, James B. Hoelzle, Kathryn A. McGuire, Amanda G. Ferrier-Auerbach, Molly J. Charlesworth, and Scott R. Sponheim. Neuropsychological evaluation of blast-related concussion: Illustrating the challenges and complexities through OEF/OIF case studies. *Brain Injury*, 25(5):511–525, May 2011. ISSN 0269-9052. doi: 10.3109/02699052.2011.558040. URL https://doi.org/10.3109/02699052.2011.558040. Publisher: Taylor & Francis _eprint: https://doi.org/10.3109/02699052.2011.558040.

Michael A. Nitsche, Leonardo G. Cohen, Eric M. Wassermann, Alberto Priori, Nicolas Lang, Andrea Antal, Walter Paulus, Friedhelm Hummel, Paulo S. Boggio, Felipe Fregni, and Alvaro Pascual-Leone. Transcranial direct current stimulation: State of the art 2008. *Brain Stimulation*, 1(3):206–223, July 2008. ISSN 1876-4754. doi: 10.1016/j.brs.2008.06.004.

Paul L. Nunez and Ramesh Srinivasan. *Electric fields of the brain: the neurophysics of EEG*. Oxford University Press, Oxford ; New York, 2nd ed edition, 2006. ISBN 978-0-19-505038-7. OCLC: ocm58451867.

Paul L. Nunez, Ramesh Srinivasan, Andrew F. Westdorp, Ranjith S. Wijesinghe, Don M. Tucker, Richard B. Silberstein, and Peter J. Cadusch. EEG coherency: I: statistics, reference electrode, volume conduction, Laplacians, cortical imaging, and interpretation

at multiple scales. *Electroencephalography and Clinical Neurophysiology*, 103(5):499–515, November 1997. ISSN 0013-4694. doi: 10.1016/S0013-4694(97)00066-7. URL https://www.sciencedirect.com/science/article/pii/S0013469497000667.

F. Perrin, J. Pernier, O. Bertrand, and J. F. Echallier. Spherical splines for scalp potential and current density mapping. *Electroencephalography and Clinical Neurophysiology*, 72 (2):184–187, February 1989. ISSN 0013-4694. doi: 10.1016/0013-4694(89)90180-6. URL https://www.sciencedirect.com/science/article/pii/0013469489901806.

Luca Pion-Tonachini, Ken Kreutz-Delgado, and Scott Makeig. ICLabel: An automated electroencephalographic independent component classifier, dataset, and website. *NeuroImage*, 198:181–197, September 2019. ISSN 1053-8119. doi: 10.1016/j.neuroimage.2019.05.026. URL http://www.sciencedirect.com/science/article/pii/S1053811919304185.

Joseph D Ramsey, Stephen José Hanson, Catherine Hanson, Yaroslav O Halchenko, Russell A Poldrack, and Clark Glymour. Six problems for causal inference from fmri. *neuroimage*, 49(2):1545–1558, 2010.

Eric Rawls, Erich Kummerfeld, Bryon A. Mueller, Sisi Ma, and Anna Zilverstand. The Resting-State Causal Human Connectome is Characterized by Hub Connectivity of Executive and Attentional Networks. *NeuroImage*, page 119211, April 2022. ISSN 1053-8119. doi: 10.1016/j.neuroimage.2022.119211. URL https://www.sciencedirect.com/science/article/pii/S1053811922003354.

Jakob Runge, Peer Nowack, Marlene Kretschmer, Seth Flaxman, and Dino Sejdinovic. Detecting and quantifying causal associations in large nonlinear time series datasets. *Science advances*, 5(11):eaau4996, 2019.

Thomas Schreiber. Measuring Information Transfer. *Physical Review Letters*, 85(2):461–464, July 2000. doi: 10.1103/PhysRevLett.85.461. URL https://link.aps.org/doi/10.1103/PhysRevLett.85.461. Publisher: American Physical Society.

Gideon Schwarz. Estimating the dimension of a model. *The annals of statistics*, pages 461–464, 1978.

Ohidul Siddiqui. MMRM versus MI in Dealing with Missing Data—A Comparison Based on 25 NDA Data Sets. *Journal of Biopharmaceutical Statistics*, 21(3): 423–436, March 2011. ISSN 1054-3406. doi: 10.1080/10543401003777995. URL https://doi.org/10.1080/10543401003777995. Publisher: Taylor & Francis _eprint: https://doi.org/10.1080/10543401003777995.

Jasmine Song, Colin Davey, Catherine Poulsen, Phan Luu, Sergei Turovets, Erik Anderson, Kai Li, and Don Tucker. Eeg source localization: Sensor density and head surface coverage. *Journal of neuroscience methods*, 256:9–21, 2015.

François Tadel, Sylvain Baillet, John C Mosher, Dimitrios Pantazis, and Richard M Leahy. Brainstorm: a user-friendly application for meg/eeg analysis. *Computational intelligence and neuroscience*, 2011:1–13, 2011.

Peter J. Uhlhaas and Wolf Singer. Neural Synchrony in Brain Disorders: Relevance for Cognitive Dysfunctions and Pathophysiology. *Neuron*, 52(1):155–168, October 2006. ISSN 0896-6273. doi: 10.1016/j.neuron.2006.09.020. URL https://www.sciencedirect.com/science/article/pii/S0896627306007276.

Lawrence M. Ward. Synchronous neural oscillations and cognitive processes. *Trends in Cognitive Sciences*, 7(12):553–559, December 2003. ISSN 1364-6613. doi: 10.1016/j.tics.2003.10.012. URL https://www.sciencedirect.com/science/article/pii/S1364661303002894.

Luc Edward Wilson, Jason da Silva Castanheira, and Sylvain Baillet. Time-resolved parameterization of aperiodic and periodic brain activity. *eLife*, 11:e77348, September 2022. ISSN 2050-084X. doi: 10.7554/eLife.77348. URL https://doi.org/10.7554/eLife.77348. Publisher: eLife Sciences Publications, Ltd.